Orientational instabilities in Couette flow of non-flow-aligning nematic liquid crystals

Ignacio Zúñiga
Departamento de Física Fundamental, Universidad Nacional de Educación a Distancia, Apartado 60141, 28080 Madrid, Spain
(Received 9 January 1989; revised manuscript received 26 September 1989)

A numerical solution of the continuum equations for nonaligning nematic liquid crystals in cylindrical Couette flow is obtained. The initial orientation of the director is radial and therefore contained in the plane of the shear. The stability of the solution is analyzed for a series of sets of material constants in order to investigate the dependence of the stability threshold with temperature. The results are compared with experiments.

I. INTRODUCTION

It is well known that in liquid crystals the orientation of the molecules is coupled to the macroscopic velocity through viscous torques. In simple shearing flow, when the alignment lies in the plane defined by the velocity vector and the velocity gradient (we refer to this plane as the shear plane), there is an equilibrium position at which the viscous and elastic torques balance. With an increase of the local shear stress, the preferred orientation tends to align in the flow at a certain angle θ_0 to the stream lines.[1] However, this situation can occur only when the Leslie viscosity coefficients α_2 and α_3 are negative. In Poiseuille flow experiments with *p*-*n*-hexyl-oxybenzylidene-*p*'-aminobenzonitrile (HBAB), Gähwiller[2] observed that below a certain temperature the coefficient α_3 becomes positive and a turbulent state develops instead of the expected flow alignment. After some dispute,[3] Pieranski and Guyon[4] measured α_3 in plane shear flow with HBAB and showed that α_3 did change sign at a certain temperature. They analyzed these new instabilities with two different configurations. In the first one, the director at both bounding plates is aligned orthogonal to the plane of shear. When α_3 is positive and the shear rate is increased beyond a critical value, a cellular (or rolls) instability was observed, with the axis of the rolls parallel to the velocity. In the other geometry, the director at the plates is aligned parallel to the velocity so that the director lies in the shear plane; we shall refer to this as planar orientation. They found that at a certain shear rate the director turns out of the plane of shear. They did not report the critical value for the instability, but they found that for sufficiently large shear rate ($s=1$ sec^{-1} for a 0.19-mm-width sample), the director is practically perpendicular to the plane of the shear. With a further increase of the shear rate ($s=4$ sec^{-1}) a cellular instability was also observed.

Using the same geometry, the same material (HBAB), and planar configuration, Pieranski, Guyon, and Pikin[5] measured the variation of the tilt angle θ with the velocity of the upper plate. They found again that for velocities larger than a critical value the director tumbles to a new state which involves the director out of the plane.

Cladis and Torza[6] studied Couette flow of HBAB and of *p*-cyanobenzilidene-*p*'-octylaniline (CBOOA), choosing for each fluid a temperature range where α_3 is positive. In the experiment, both cylinders were made out of glass so that a polarizing microscope could be used to observe directly the director orientation. As they fixed homeotropic orientation at the walls, the director aligns along the radial direction when both cylinders are at rest. Flow was generated by rotating the inner cylinder, with the outer one fixed. As the angular velocity of the inner cylinder was increased, three distinct regimes were observed. In the first, the director and velocity vectors are contained in the plane of the shear. The shear stress tilts the director from its orientation at the walls ($\theta=0$) to a maximum angle θ_m somewhere in the gap. When θ_m is about $-\pi/2$, an instability occurred and the system jumped to a new state. In this new state, θ_m is smaller than $-\pi$. This first instability was called "tumbling," and two regions were observed in the gap where the director is radial, i.e., $\theta=-\pi$ (tumbling lines). Although across most of the gap the director remains in the shear plane, there are two layers near the walls where the director is oriented axially. In spite of the different initial orientations (planar in Ref. 4 and homeotropic in Ref. 6), the different geometry (plane shear flow[4] and cylindrical Couette flow[6]) and the above-mentioned layers near the walls, Cladis and Torza[6] claimed that their results are in contrast with those of Pieranski and Guyon,[4] who did not observe, after the first instability, a stable solution with the director in the plane.

Increasing the shear rate, Cladis and Torza[6] found a second instability leading to a third regime where they observed rolls. They also studied the variations of both thresholds with temperature. The first threshold behaves in the same way for both nematics. Its value diverges as the temperature increases to a certain value at which $\alpha_3=0$. The second threshold shows behavior for HBAB different from that for CBOOA. For CBOOA, starting at a temperature of about 100 °C (at which α_3 just becomes positive) and decreasing the temperature, they found the threshold diverges as α_3 approaches $|\alpha_2|$, so that for temperatures below $T=88$ °C, the instability does not occur and therefore the second regime is stable to the highest shear rate used. All this is in contrast with the threshold measured for HBAB, which is almost constant in the range of temperatures used in the experiment. These

different behaviors are due to the fact that CBOOA presents a nematic–smectic-A transition. It was predicted by Jähnig and Brochard[7] that, near such a phase transition, α_3 diverges to $+\infty$.

In a later experiment, Pieranski and Guyon[8] also used CBOOA to investigate the instability of plane shear flow. They discussed very briefly the case where the director is fixed at the boundaries parallel to the velocity because the results are similar to those with HBAB,[4] namely that, when α_3 is positive beyond the first instability, the director is out of the plane. They also studied the case where the director is initially orthogonal to the plane of the shear and it was found that the threshold for cellular instability behaves with temperature in the same way as the corresponding one in the experiments of Cladis and Torza,[6] i.e., the cellular instability occurs only in the range of temperatures at which α_3 is positive but smaller than $|\alpha_2|$, and the threshold diverges as α_3 approaches $|\alpha_2|$. Based on the above similarities, the authors pointed out that in spite of the different orientation of the director at the boundaries (planar in Ref. 4 and homeotropic in Ref. 6), the cellular instability observed in both experiments would be of the same nature if the director aligned orthogonal to the plane of the shear in most of the gap.

The theoretical studies are very much behind experiments. Cladis and Torza[6] presented approximate analyses of instabilities in an attempt to interpret their observations more fully, while earlier papers by de Gennes[9] and Pikin[10] also discussed this topic. Manneville[11] considered plane shear flow with the initial assumption that the director remains in the plane of shear. By numerical integration of the two-dimensional equations it was found that the maximum value of the tilt angle θ_m is a multivalued function of the shearing velocity V. Manneville then explained the tumbling as a discontinuous jump from one branch to another. Subsequently, Carlsson,[12] also by numerical integration of simplified continuum equations, showed that the function $\theta_m(V)$ is multivalued only for small negative values of the ratio α_3/α_2.

However, in order to explain an instability with the director out of the plane of the shear, it is necessary to consider three-dimensional equations. With simplified equations only valid for small distortion about planar orientation, Pieranski, Guyon, and Pikin[5] suggested that there are two different instabilities: one in the shear plane and another taking the director out of the shear plane. However, both corresponding thresholds are so close to each other that the former is concealed by the latter. Carlsson[13] studied the stability of plane shear flow but neglected transverse flow effects. According to his analysis the anchoring of the director at the walls can explain both experimental findings. In the case of planar boundary conditions, the instability is first out of the shear plane, but with a homeotropic boundary conditions is first in the shear plane. This is in contrast with results in plane shear flow obtained by Zúñiga and Leslie.[14] They obtained a numerical solution of the full equations and examined its stability to perturbations both in and out of the plane of shear. They concluded that, at least for the series of sets of material constants they have studied, the solution after the first instability always involves the director out of the plane and this result is independent of whether the initial alignment is planar or homeotropic.

Homeotropic orientation was also considered in experiments by Hiltrop and Fisher.[15] They studied the flow of a layer of p'-methoxybenzylidene-p-n-butylaniline (MBBA) in radial Poiseuille flow. Using basically the same optical technique as Cladis and Torza, three consecutive deformation modes of the director were found. In the first and in the third mode the director is contained into the shear plane, but in the second mode the director comes out of the shear plane. Zúñiga and Leslie[16] studied the stability of numerical solutions describing first and third mode. They calculated the critical pressure drop at which the first mode becomes unstable to perturbations out of the shear plane, while the third mode is stable to the highest pressure drop they considered.

In this paper we solve numerically continuum equations for nematics in cylindrical Couette flow. The stability of the solution is analyzed in order to investigate whether the rotation and the cylindrical geometry of the Couette could be the reason why the flow is different from plane shear flow and Poiseuille flow. In the next section the relevant continuum equations for this problem are discussed. A derivation of the equations is given in the Appendix. In Sec. III a numerical solution of the basic steady flow is computed and described. The stability of the solution is analyzed in Sec. IV, and some conclusive remarks are presented in Sec. V.

II. BASIC EQUATIONS

Consider flow between two concentric circular cylinders of radii R_1 and R_2 ($R_1<R_2$), which are rotating with constant angular velocities Ω_1 and Ω_2, respectively. Cylindrical polar coordinates r, ψ, and z are chosen such that the z axis is parallel to the common axis of the cylinders. With this choice we consider the physical components of the velocity $\mathbf{v}$ and the director $\mathbf{n}$ to be of the following forms:

$$v_r=0,\quad v_\psi=r\omega(r,t),\quad v_z=v(r,t)\ ,$$
$$n_r=\sin\theta\cos\phi,\quad n_\psi=\cos\theta\cos\phi,\quad n_z=\sin\phi\ , \tag{1}$$

where θ and ϕ are also functions of r and t. We only consider r and t dependence because experimental observations[6] showed that the first instability led to a state invariant along ψ and z. Therefore this analysis is not valid for the rolls regime observed beyond a subsequent instability.

A derivation of continuum equations for nematics in this geometry is given in the Appendix. After being linearized with respect to v, ϕ, and $\dot\theta$, the equations reduce to

$$\left[r\left[\omega' g(\theta)+\frac{1}{2r}\dot\theta(\gamma_1+\gamma_2\cos2\theta\right]\right]' +2\left[\omega' g(\theta)+\frac{1}{2r}\dot\theta(\gamma_1+\gamma_2\cos2\theta\right]=\rho r\dot\omega\ , \tag{2}$$

$$[v'g_1(\theta)+r\omega'g_2(\theta)\phi+\dot{\phi}\alpha_2\sin\theta]'$$
$$+\frac{1}{r}[v'g_1(\theta)+r\omega'g_2(\theta)\phi+\dot{\phi}\alpha_2\sin\theta]=\rho\dot{v} , \quad (3)$$

$$2f(\theta)\left[\theta''+\frac{1}{r}\theta'\right]+\frac{df(\theta)}{d\theta}\left[(\theta')^2+\frac{1}{r^2}\right]$$
$$-r\omega'(\gamma_1+\gamma_2\cos2\theta)-2\gamma_1\dot{\theta}=0 , \quad (4)$$

$$f_1(\theta)\phi''+\left[\frac{df_1(\theta)}{dr}+\frac{1}{r}f_1(r)\right]\phi'+\left[f_2+\frac{\gamma_2}{2}r\omega'\sin2\theta\right]\phi$$
$$-\frac{\gamma_2-\gamma_1}{2}v'\sin\theta-\gamma_1\dot{\phi}=0 , \quad (5)$$

where the superposed dot denotes $\partial/\partial t$, the prime denotes $\partial/\partial r$,

$$2g_1(\theta)=\alpha_4+(\alpha_5-\alpha_2)\sin^2\theta ,$$
$$2g_2(\theta)=(2\alpha_1\sin^2\theta+\alpha_3+\alpha_6)\cos\theta ,$$
$$g(\theta)=g_1(\theta)+g_2(\theta)\cos\theta ,$$
$$\gamma_1=\alpha_3-\alpha_2, \quad \gamma_2=\alpha_6-\alpha_5=\alpha_2+\alpha_3 ,$$

α_1 to α_6 are viscosity coefficients,

$$f(\theta)=K_1\cos^2\theta+K_3\sin^2\theta ,$$
$$f_1(\theta)=K_2+(K_3-K_2)\sin^2\theta ,$$
$$f_2=\theta''(K_2-K_1)\tfrac{1}{2}\sin2\theta$$
$$+(\theta')^2[K_2-(3K_2-K_1-2K_3)\sin^2\theta]$$
$$+\frac{\theta'}{2r}(5K_2-4K_3-K_1)\sin2\theta$$
$$+\frac{1}{r^2}[K_1-(K_1+K_2-2K_3)\cos^2\theta] ,$$

and K_1, K_2, and K_3 are elastic constants.

Equations (2) and (3) express the conservation of the components of linear momentum along the ψ and z axis, respectively. In the viscous forces, on the left-hand side of both equations, there are two kind of terms. Those proportional to velocity derivatives are the anisotropic extension to the viscous terms in isotropic fluids [the viscosity instead of a constant is now a function $g(\theta)$]. The second kind of terms that are peculiar to nematics represent contributions due to nonuniform orientation of the director. Note that the coefficients of both differential equations are variables because the initial alignment is nonuniformly distorted by the flow. Consequently, no simple solution of the equations can be found analytically. This is in contrast with the particular configuration where the initial orientation of the director is parallel to the cylindrical axis, i.e., perpendicular to shear plane. In that configuration the flow does not distort the director and the nematic behaves as a Newtonian fluid with viscosity $\alpha_4/2$. In that configuration, as the shear rate is increased, another interesting series of instabilities is found.[17]

Angular momentum conservation is expressed in Eqs. (4) and (5). Each term can be seen as a torque exerted on the director. Terms involving functions f, f_1, and f_2 are elastic torques associated with distortions of the director field, while those involving velocity derivatives are viscous torques coupling velocity and director fields. Finally, the viscous damping terms are proportional to the $\dot{\theta}$ and $\dot{\phi}$.

Equation (4) gives the dynamic equilibrium of the projection of the torques in the plane of shear. A certain shear rate ω' induces through the viscous torques a deformation of the director field. As a result of the deformation there is an elastic torque of opposite sign until an equilibrium position is reached. However, if the deformation is such that $\pi<\theta<3\pi/2$, both elastic and viscous torques are of the same sign and the director tumbles.

Equation (5) gives the dynamic equilibrium among torques associated with distortions of the director out of the shear plane. In this geometry for slow shear rates the director and the applied velocity are contained in the plane of shear ($\phi=v=0$) and the equation is satisfied. Note that in addition to the viscous torque associated with velocity perturbations v' in the z direction there is also a term proportional to the applied shear velocity ω'. The elastic torques depend now on the twist elastic constant K_2 as expected, but they also depend on the director splay-bend distortion in the plane of shear. At low shearing rates small perturbations of ϕ and v are damped. For high enough shearing rates the total torque changes sign and the perturbations out of the plane will grow. Fischer,[18] considering a model with pure splay-bend, i.e., no flow and no twist, found a critical deformation beyond which the director comes out of the plane.

With the assumption that there is strong anchoring at the cylinders, we take the boundary conditions on the director to be

$$\theta(R_1)=\theta_w, \quad \theta(R_2)=\theta_w+n\pi ,$$
$$\phi(R_1)=\phi_w, \quad \phi(R_2)=\phi_w+m\pi , \quad (6)$$

where m and n are integers. It is clear that we can find a different solution for each value of m and n. However, here we consider only the case where the initial alignment is radial with $\theta_w=\pi/2$, $\psi_w=0$, $m=0$, $n=0$. The solution with $n=1$, for instance, represents the director undergoing a net rotation of π between the boundaries.

In addition, the usual no-slip condition gives

$$\omega(R_1)=\Omega_1, \quad \omega(R_2)=\Omega_2, \quad v(R_1)=v(R_2)=0 , \quad (7)$$

and we take $\Omega_2=0$. This choice of boundary conditions corresponds to the experiments of Cladis and Torza.[6]

III. STEADY SOLUTION

In view of the boundary conditions (6) and (7), and for sufficiently small values of the angular velocity Ω_1 of the inner cylinder, one expects that there will be a steady state in which the director remains in the r-ψ plane with no axial velocity, i.e., v and ϕ are both zero. In this event, Eq. (2) reduces to

$$[r\omega'g(\theta)]'+2\omega'g(\theta)=0 , \quad (8)$$

and thus

$$r^3\omega' g(\theta)=c \ , \tag{9}$$

where c is a positive constant equal to the couple per unit length on either cylinder. With (9), Eq. (4) may now be written

$$2f(\theta)(r^2\theta''+r\theta')+\frac{df(\theta)}{d\theta}[r^2(\theta')^2+1] - \frac{c}{g(\theta)}(\gamma_1+\gamma_2\cos 2\theta)=0 \ . \tag{10}$$

An analysis of the above equations when the viscosity coefficient α_3 is negative was done by Atkin and Leslie.[19] They showed that there is a solution in which the director rotates from $\theta_w=0$ at one boundary to a maximum value θ_m somewhere in the gap, and then, reversing the direction of rotation, returns to the value θ_w at the other boundary. For larger shear rates, θ_m tends to the Leslie angle $\theta_0=\frac{1}{2}\tan^{-1}(\alpha_3/\alpha_2)^{1/2}$ in the gap, except for thin layers at the walls.

However, when α_3 is positive, θ_m increases without limit as c is increased. In this case it is necessary to solve Eqs. (9) and (10) numerically. For a given value of c, we determine $\theta(r)$ from (10) and then $\omega(r)$ from (9).

The computation was performed using dimensionless equations. We used the radius R_1 as the natural length scale and $\gamma_1 R_1^2/K_1$ as the time scale. The equations would read exactly as they are written if we make the following substitutions:

$$(\hat{f},\hat{f}_1)=(f,f_1)/K_1, \quad \hat{f}_2=R_1^2 f_2/K_1 \ ,$$

$$(\hat{g},\hat{g}_1,\hat{g}_2)=(g,g_1,g_2)/\gamma_1 \ ,$$

$$A=c/K_1, \quad E_r=\gamma_1 R_1^2\Omega_1/K_1 \ .$$

We rename all the dimensionless quantities without the hat, but we keep A for the dimensionless couple per unit length and the so-called Ericksen number E_r for the dimensionless angular velocity of the outer cylinder.

The solution is plotted in Figs. 1 and 2 for two different values of A. We use a set of material constants with $\alpha_3/|\alpha_2|=0.05$ (set 3 of Table I); this corresponds approximately to HBAB at 85 °C, which was used in the experiments of Cladis and Torza.[6] In Fig. 3 the difference between the velocity profile v_I of a Newtonian fluid and the velocity profile v_N of a nematic is shown. The difference v_N-v_I has two stationary values, one near each wall. Near the inner wall the nematic moves faster than the equivalent Newtonian fluid, whereas near the other wall the nematic moves slower. However, the maximum difference in the velocities is only about 0.15% of the actual velocity, and therefore, in most of the gap, the flow can be considered to be nearly Newtonian. All this is in qualitative agreement with experimental findings.[6] A closer comparison is impossible for two reasons: first, because we have used for the computation values of the ma-

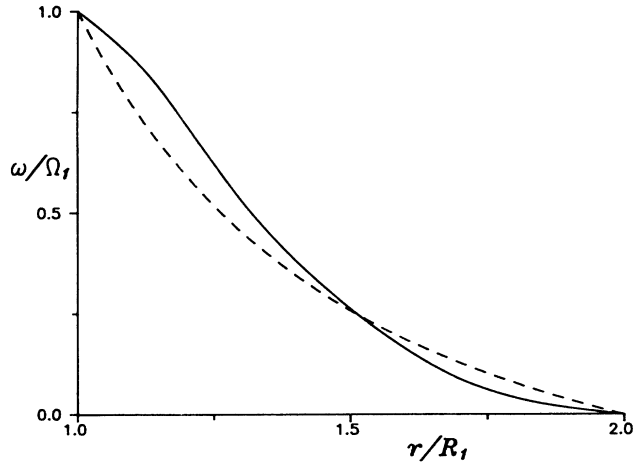

FIG. 2. The solid line corresponds to the dimensionless velocity profile of the nematic across the gap just below the first instability. Set 3 of material constants $A=140$ and $R=2$ were used in the computation. The dashed line corresponds to the profile of an isotropic fluid.

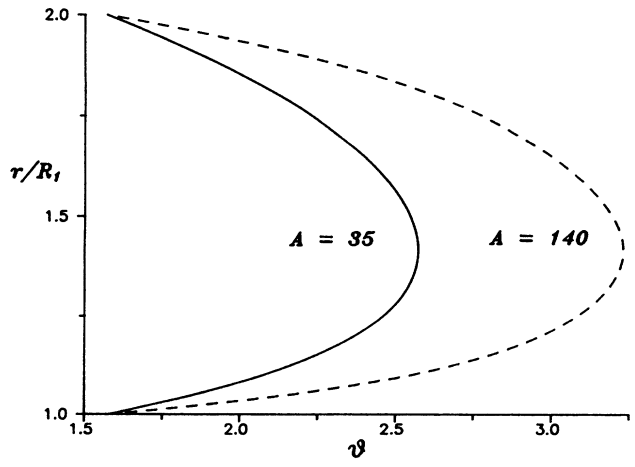

FIG. 1. Tilt angle across the gap for two different values of the dimensionless couple per unit length A exerted on each cylinder. The calculation was performed using set 3 of material constants and a ratio between cylinders $R=2$.

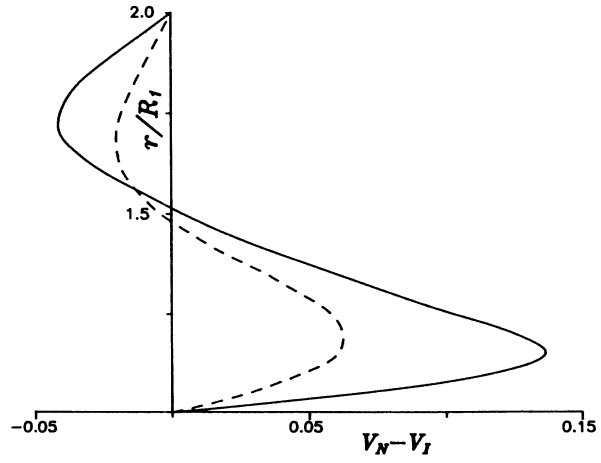

FIG. 3. Difference between the velocity of an isotropic fluid v_I and that v_N for a nematic liquid crystal, for two values of the dimensionless couple A. It shows how the nematic moves faster near the inner wall and it moves slower near the outer wall.

TABLE I. Numerical values of viscosities and elastic constants of 8CBP. All viscosity values are in Pa s and elastic constants in N. The values are taken from Refs. 24–27. Unfortunately, we have not found complete sets of viscosities and elastic constants of HBAB or CBOOA in the range of temperature at which α_3 is positive. In sets 2 and 4 the values of γ_1 have been slightly modified in order to obtain positive values of α_3 and intermediate values of ϵ. The results show that the important parameter of the problem is the ratio ϵ and are not very sensitive to variations of the other constants.

Set	1	2	3	4	5	6
α_1	0.026	0.014	0.038	0.0078	0.134	0.39
$-\alpha_2$	0.052	0.049	0.059	0.045	0.070	0.070
α_3	0.825×10^{-3}	0.15×10^{-2}	0.305×10^{-2}	0.42×10^{-2}	0.014	0.027
α_4	0.050	0.049	0.052	0.048	0.056	0.057
α_5	0.043	0.036	0.047	0.026	0.053	0.059
α_6	-0.82×10^{-2}	−0.011	-0.84×10^{-2}	−0.014	-0.29×10^{-2}	0.016
$K_1(10^{11})$	1.29	0.90	1.20	0.70	1.40	1.45
$K_2(10^{11})$	0.60	0.40	0.56	0.35	0.70	0.90
$K_3(10^{11})$	1.30	0.90	1.20	0.67	2.10	2.80
ϵ	0.016	0.031	0.052	0.094	0.2	0.39

terial constants corresponding to 4-*n*-octyl-4′-cyanobiphenyl (8CBP) (see Table I), and second, because the velocity profile given in Fig. 1 of Ref. 6 seems to have been measured at a shear rate well beyond the occurrence of the first instability[21] and therefore it is outside the scope of the present analysis.

The integration was achieved by means of a NAG routine[20] based on finite difference technique with deferred correction and Newton iteration. The routine, supplied with an initial "guess" for the profiles $\theta(r)$ and $\omega(r)$, finds a solution satisfying the boundary conditions. In principle, increasing the absolute error tolerance and the number of mesh points, the solution could be obtained at any desired accuracy compatible with the roundoff error of the computer. However, there is a critical value of A (point P_1 in Fig. 4) at which the solution seems to disappear. For values of A higher than the critical one, a second solution (point P_2 in Fig. 4) characterized by a much higher distortion is found. There is a kind of numerical instability associated with this point and a very good estimate of the solution is required by the procedure to converge. Using the second solution as initial guess and either increasing or decreasing A, one can explore the range (region III in Fig. 4) at which the solution exists. There is an intermediate region (region II) between P_1 and P_3 where a third solution can be found. In the case of plane shear flow, Carlsson[12] computed the dissipation energy of each solution, showing that in the range of values of A at which there is more than one solution, the minimum dissipation energy corresponds to that involving the smallest director distortion.

IV. STABILIY ANALYSIS

Experimental observations suggest that when the above steady flow first becomes unstable, the perturbations are independent of the axial coordinate z and have a nonoscillatory growth in time t. Therefore we consider perturbations of the form

$$(\tilde{\omega},\tilde{v},\tilde{\theta},\tilde{\phi})=(\Omega(r),V(r),\Theta(r),\Phi(r))e^{-\sigma t}\,, \tag{11}$$

where σ is real. We substitute the perturbed solution $(\omega+\tilde{\omega},\tilde{v},\theta+\tilde{\theta},\tilde{\phi})$ into Eqs. (2)–(5) and neglect second-order terms in the perturbations. We also neglect inertia terms proportional to $\dot{\omega}$ and $\dot{v}$. We thus obtain two uncoupled equations for the perturbations $\tilde{\theta}$ in the plane of the shear and $\tilde{\phi}$ out of the plane of the shear:

$$f_1(\theta)\Phi''+\Phi'\left[\frac{1}{r}f_1(\theta)+\theta'\frac{df_1(\theta)}{d\theta}\right]+\Phi\left[f_2+\frac{A\sin\theta}{r^2g(\theta)}\left[\lambda\cos\theta+\frac{\alpha_2g_2(\theta)}{\gamma_1g_1(\theta)}\right]\right]+\sigma_o\Phi\left[1-\left[\frac{\alpha_2}{\gamma_1}\sin\theta\right]^2\frac{1}{g_1(\theta)}\right]=0\,, \tag{12}$$

$$f(\theta)\Theta''+\Theta'\left[\frac{1}{r}f(\theta)+\theta'\frac{df(\theta)}{d\theta}\right]+\Theta\left\{\left[\frac{df(\theta)}{d\theta}\left[\theta''+\frac{1}{r}\theta'\right]+\frac{1}{2}\frac{d^2f(\theta)}{d\theta^2}\left[(\theta')^2+\frac{1}{r^2}\right]\right]\right.$$
$$\left.+\frac{A}{2r^2g(\theta)}\left[2\lambda\sin2\theta+(1+\lambda\cos2\theta)\frac{1}{g(\theta)}\frac{dg(\theta)}{d\theta}\right]\right\}+\sigma_i\Theta\left[1-\frac{1}{4g(\theta)}(1+\lambda\cos2\theta)^2\right]=0\,, \tag{13}$$

with $\lambda=\gamma_2/\gamma_1$. We consider strong anchoring of the director at the walls and therefore we impose the following boundary conditions for the perturbations:

$$\Phi=\Theta=0 \quad \text{at } r=R_1,R_2\,. \tag{14}$$

Due to the fact that Eqs. (12) and (13) are uncoupled, they define two independent neutral stability thresholds. For a given value of the couple A we determine the steady solution from (9) and (10), and then we solve the

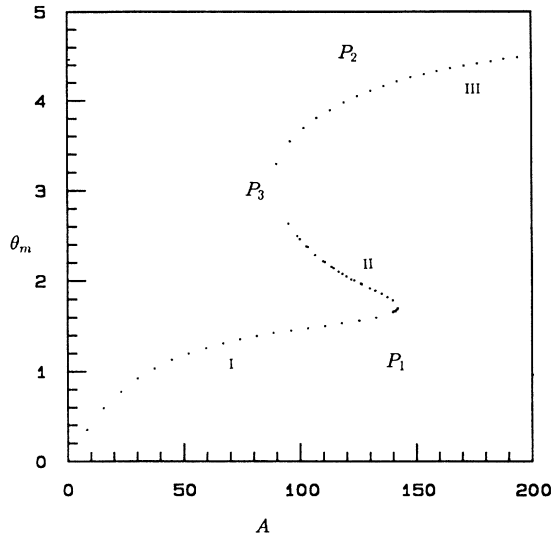

FIG. 4. Maximum tilt angle θ_m vs the dimensionless couple A. The calculation was performed with set 3 of material constants.

eigenvalue problems (12)–(14) to compute σ_o and σ_i as the eigenvalues. The steady solution will be unstable to perturbations out of the shear plane if σ_o is negative and will be unstable to perturbations in the shear plane if σ_i is negative.

All this analysis is somewhat similar to the equivalent one for plane shear flow when α_3 is negative (Currie and MacSithigh[22]) and when α_3 is positive (Zúñiga and Leslie[14]), except that now the equations governing the perturbations are not of the Sturm-Liouville type. This fact does not make much difference from a numerical point of view, as we use a general technique for two-point boundary-value problems based on a shooting and matching method.[23] As we mentioned before, there are some difficulties for calculating the basic solution near a critical value of the shear rate at which the solution seems to disappear. Such a critical value is very close to the one at which the solution becomes unstable to perturbations in the shear plane. In the case where the solution is first unstable to perturbations out of the plane the basic solution can be easily calculated and the threshold is found at the required accuracy. However, this is not the case when either both thresholds are very close to each other or the solution is first unstable to perturbations in the shear plane. In those cases the threshold for instability out of the shear plane has to be found by interpolation.

The computational results are summarized in Table II. They differ only very little from those in plane shear flow,[14] and therefore suggest that the rotation and cylindrical geometry have only a small effect on the first threshold. In different geometry a complete comparison between the hydrodynamic instabilities in Couette flow in isotropic fluids and those of nematics is given by Dubois-Violette and Manneville.[17] The cylindrical geometry is stabilizing in the sense that the director achieves a bigger value of θ_m before the solution becomes unstable. For the data sets 1–5 (Table I) the threshold for instability out of the plane is always smaller than that for instability in the plane. For set 6 (which may well be out of the range of temperatures at which the experiments were performed) the instability in the plane takes place first, but the director tumbles to a new state that is already unstable to perturbations out of the plane (see caption of Table II). As we discussed above we have computed the solution beyond the first instability, regions II and III in Fig. 4. Although linear stability analysis is only valid for small perturbations, we have studied the stability of the solution in the three regions. In region II the solution is always unstable. In region III the solution is stable. This result is in contrast with that found for plane shear flow where the solution beyond the first instability was always unstable to perturbations out of the plane. In Fig. 5 the eigenfunction $\phi(r)$ in the three regions when $A=130$ is plotted. The dotted line corresponds to the eigenfunction before the first instability, region I. The eigenfunction

TABLE II. Maximum distortion angle $\beta_m=\theta_m-\theta_w$, critical Eriksen number and dimensionless couple for different sets of material constants. The computation was performed using $R=R_2/R_1=2$. With set 6 the solution tumbles from $\beta_m=77.0°$ to $\beta_m=105.4°$, but it is unstable to perturbations out of the plane of shear since $\beta_m=103.1°$.

Set	ϵ	β_m^{in}	β_m^{out}	E_r	$-A$
1	−0.0163	94.14	94.01	208.5	291.0
2	−0.0937	95.85	95.28	141.0	194.0
3	−0.0519	97.97	96.83	101.2	142.0
4	−0.0930	102.0	99.69	70.3	96.6
5	−0.2000	138.6	101.4	48.3	80.9
6	−0.3870	77.0	103.1	25.45	92.0

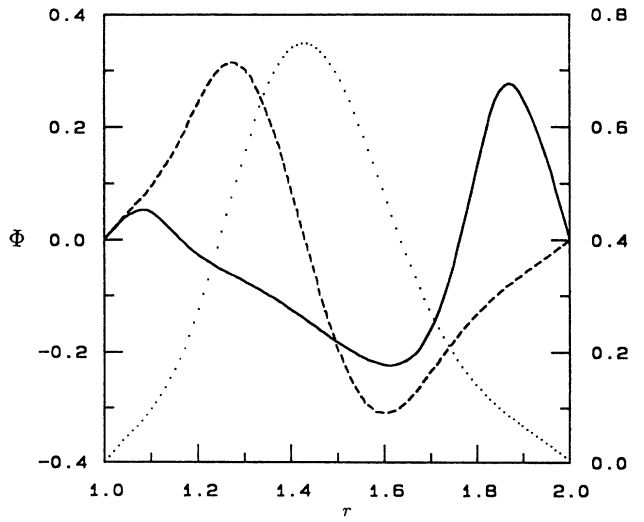

FIG. 5. Eigenfunction $\phi(r)$ at $A=130$. Dotted line corresponds to the solution with the smallest deformation, region I. The dashed line corresponds to the intermediate deformation, region II; and the solid line to the largest deformation, region III.

shows one maximum near the center of the gap. The solid line corresponds to the eigenfunction after the instability, region III. There are now two maxima near the boundaries that may resemble the two observed layers[6] where the director has a nonzero axial component. It is possible that after the first instability the director somehow comes back to the shear plane and the solution adopted by the system is the corresponding to region III. The shape of the eigenfunction gives an idea of the critical mode. So one expects that in the first instability the director comes out of the shear plane mainly in the middle of the gap. During the transition, region II, the director is twisted in one direction in one half of the gap and in the opposite direction in the other half. Finally, in region III, the shape of the eigenfunction suggests that in the next instability the director will come out of the plane mainly near the boundaries. This could be an explanation of experimental findings, but it is only a conjecture as we are neglecting nonlinear terms in ϕ and v.

In Fig. 6 the critical velocity corresponding to the first instability is plotted as a function of the ratio α_3/α_2, which we denote by ϵ. We also plot the experimental results given in Fig. 2(a) of Ref. 6. In spite of the different scales used at the axes and the fact that we are using values for a different material, the agreement with experiments is fairly good. In the experiment the estimated value for ϵ is 0.06 for HBAB at 85 °C and, using $R_2/R_1 \approx 3$ with $R_1 = 0.16$, the critical velocity was found to be $\omega_c \approx 0.07$ rev/sec. Our result for data set 3 is $\omega_c = (K_1/\gamma_1 R_1^2)(E_r/2\pi) = (46\times 10^{-3})/2.03 = 0.025$ rev/sec. This value lies between $\omega_c \approx 0.07$ for HBAB and $\omega_c \approx 0.02$ for CBOOA at the same temperature.

In order to investigate the effect of the curvature on the stability, we have compared the critical angular velocity for different values of the ratio $R = R_1/R_2$. Interestingly, we find that the product of the critical angular velocity with the gap width is almost constant (see Table III).

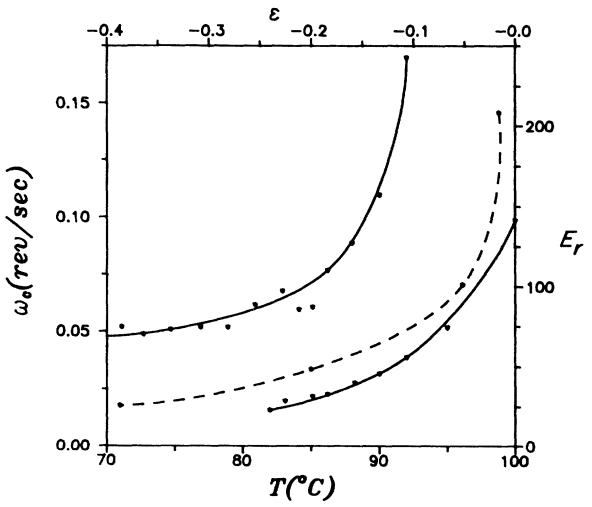

FIG. 6. The dashed line is the nondimensional critical angular velocity E_r for the first instability as a function of $\epsilon = \alpha_3/\alpha_2$. The points used to interpolate the curve are those given in Table I. Both solid lines are experimental measurements of critical angular velocity ω_c vs temperature (Ref. 6). The upper one corresponds to HBAB and the lower to CBOOA.

TABLE III. Critical angular velocity for different values of the ratio between the radii of the cylinders R. Data set 3 of constants were used in the computations.

E_r	R_2/R_1	$E_r(R_2/R_1-1)$
223	1.5	111
101	2.0	101
63	2.5	94
46	3.0	92

V. CONCLUSIONS

Steady solutions of the hydrodynamical equations for cylindrical Couette flow have been obtained numerically, and are found to be in qualitative agreement with experimental measurement of the velocity profile. The stability of the solution has also been considered, and critical values for velocity and tilt angles θ_m computed for instabilities both in the plane of shear and out of the plane of shear. Several sets of material constants have been used to investigate the effect of temperature on the critical velocity, and the results are in agreement with experiments. Couette flow instabilities in nematic liquid crystals are similar to those in plane shear because they are mainly orientational and occur at small angular velocities for which centrifugal forces are negligible.

Concerning the differences in the experimental observations between the instabilities in plane shear flow and those in Couette flow, our conclusions are very much the same as in our previous paper.[14] We find that the director comes out of the plane of shear after the first instability. This means that the transition between the first basic solution and a second solution requires some component of the director out of the shear plane. In contrast with the plane shear flow case, beyond the first instability there is a stable solution with both velocity and director fields contained in the shear plane. Assuming that the director comes back to the shear plane this latter solution could be the one observed in the experiments. However, this analysis is only valid for small perturbations of the basic solution in the plane of shear. Therefore more definitive conclusions require the consideration of nonlinear terms in the three-dimensional equations.

ACKNOWLEDGMENTS

I wish to thank Professor F. M. Leslie for suggesting this problem and both Professor F. M. Leslie and Dr. B. R. Duffy for stimulating discussions and criticisms of the manuscript. This research was partially supported by Comunidad de Madrid, Spain, while I was visiting Strathclyde University.

APPENDIX

The linear momentum equations are taken from Leslie;[1] in the present geometry they reduce to

$$\sigma'_{rr}+\frac{1}{r}(\sigma_{rr}-\sigma_{\psi\psi})-\frac{\partial p}{\partial r}=-\rho r\omega^2 , \tag{A1}$$

$$\sigma'_{r\psi}+\frac{1}{r}(\sigma_{r\psi}+\sigma_{\psi r})=\rho r\dot{\omega} , \tag{A2}$$

$$\sigma'_{rz}+\frac{1}{r}\sigma_{rz}=\rho\dot{v} . \tag{A3}$$

The stress tensor components, when linearized with respect to the variables v, ϕ, and $\dot{\theta}$, are

$$\sigma_{r\psi}=\frac{1}{r}f(\theta)\theta'-\frac{1}{2r^2}\frac{df(\theta)}{d\theta}+r\omega' g(\theta)+\tfrac{1}{2}(\gamma_1+\gamma_2\cos 2\theta)\dot{\theta} , \tag{A4}$$

$$\sigma_{\psi r}=-\frac{1}{2}\frac{df(\theta)}{d\theta}(\theta')^2+\frac{1}{r}\theta'\left[f(\theta)+\frac{1}{2}\frac{d^2f(\theta)}{d\theta^2}\right]+r\omega'[g(\theta)-\tfrac{1}{2}(\gamma_1+\gamma_2\cos 2\theta)]-[\gamma_1-\tfrac{1}{2}(\gamma_1+\gamma_2\cos 2\theta)]\dot{\theta} , \tag{A5}$$

$$\sigma_{rz}=v' g_1(\theta)+r\omega' g_2(\theta)\phi+\dot{\phi}\alpha_2\sin\theta . \tag{A6}$$

Inserting (A4)–(A6) into (A1)–(A3), one obtains Eqs. (2) and (3). For the present problem, the angular momentum equations[1] reduce to

$$g_r+\Pi'_{rr}+\frac{1}{r}(\Pi_{rr}-\Pi_{\psi\psi})+\gamma\sin\theta=0 , \tag{A7}$$

$$g_\psi+\Pi'_{r\psi}+\frac{1}{r}(\Pi_{r\psi}+\Pi_{\psi r})+\gamma\cos\theta=0 , \tag{A8}$$

$$g_z+\Pi'_{rz}+\frac{1}{r}\Pi_{rz}+\phi\gamma=0 . \tag{A9}$$

The linearized director stress tensor components are

$$\Pi_{rr}=\theta'[K_1+(K_3-K_2)\sin^2\theta]\cos\theta+[K_1-K_2-K_4-(K_3-K_2)\cos^2\theta]\frac{\sin\theta}{r} , \tag{A10}$$

$$\Pi_{r\psi}=\theta'[(K_2-K_3)\sin^2\theta-K_2]\sin\theta+[(K_3-K_2)\sin^2\theta-K_4]\frac{\cos\theta}{r} , \tag{A11}$$

$$\Pi_{\psi r}=\theta'[(K_3-K_2)\cos^2\theta-K_4]\sin\theta-[(K_3-K_2)\cos^2\theta+K_2]\frac{\cos\theta}{r} , \tag{A12}$$

$$\Pi_{\psi\psi}=\theta'[(K_1-K_2-K_4)-(K_3-K_2)\sin^2\theta]\cos\theta+[K_1+(K_3-K_2)\cos^2\theta]\frac{\sin\theta}{r} , \tag{A13}$$

$$\Pi_{rz}=\phi'[(K_3-K_2)\sin^2\theta+K_2] , \tag{A14}$$

and the linearized intrinsic-director body-force components are

$$g_r=(K_2-K_3)\left[(\theta')^2\sin\theta-\frac{1}{r}\theta'\cos\theta\right]-\gamma_1\dot{\theta}\cos\theta-\tfrac{1}{2}(\gamma_1+\gamma_2)r\omega'\cos\theta , \tag{A15}$$

$$g_\psi=(K_3-K_2)\frac{1}{r}\left[\theta'\sin\theta-\frac{1}{r}\cos\theta\right]+\gamma_1\dot{\theta}\sin\theta-\frac{\gamma_2-\gamma_1}{2}r\omega'\sin\theta , \tag{A16}$$

$$g_z=-\gamma_1\dot{\phi}-\frac{\gamma_2-\gamma_1}{2}v'\sin\theta . \tag{A17}$$

After the elimination of the director tension γ from Eqs. (A7)–(A9), one obtains Eqs. (4) and (5).

[1] F. M. Leslie, Arch. Ration. Mech. Anal. **28**, 265 (1968).

[2] Ch. Gähwiller, Phys. Rev. Lett. **28**, 1554 (1972); Mol. Cryst. Liq. Cryst. **20**, 301 (1973).

[3] S. Meiboom and R. C. Hewitt, Phys. Rev. Lett. **30**, 261 (1973); D. Forster, Phys. Rev. Lett. **35**, 1161 (1974).

[4] P. Pieranski and E. Guyon, Phys. Rev. Lett. **32**, 924 (1974).

[5] P. Pieranski, E. Guyon, and S. A. Pikin, J. Phys. (Paris) Colloq. **37**, C1-3 (1976).

[6] P. E. Cladis and S. Torza, Phys. Rev. Lett. **35**, 1283 (1975); J. Colloid Interface Sci. **4**, 487 (1976).

[7] There are several coefficients that diverge just above the transition to smectic *A*. P. G. de Gennes, Solid State Commun. **10**, 753 (1972) discusses the divergence of elastic constants K_2 and K_3. F. Jähnig and F. Brochard, J. Phys. (Paris) **35**, 301 (1974) showed that the viscosities α_1, α_3, and α_6 diverge as well.

[8] P. Pieranski and E. Guyon, Comments Phys. **1**, 45 (1976).

[9] P. G. de Gennes, Phys. Lett. **41A**, 479 (1972); *The Physics of Liquid Crystals* (Clarendon, Oxford, 1974).

[10] S. A. Pikin, Zh. Eksp. Teor. Fiz. **64**, 2495 (1973) [Sov. Phys.—JETP **38**, 1246 (1974)].

[11] P. Manneville, Mol. Cryst. Liq. Cryst. **70**, 223 (1982).

[12] T. Carlsson, Mol. Cryst. Liq. Cryst. **70**, 307 (1984).

[13] T. Carlsson, Phys. Rev. A **34**, 3393 (1986).

[14] I. Zúñiga and F. M. Leslie, Europhys. Lett. **9**, 689 (1989); Liq. Cryst. **5**, 725 (1989).

[15] K. Hiltrop and F. Fischer, Z. Naturforsch. **31A**, 800 (1976).

[16] I. Zúñiga and F. M. Leslie, Non-Newtonian Fluid Mech. **33**, 123 (1989).

[17] E. Dubois-Violette and P. Manneville, J. Fluid Mech. **89**, 273 (1978).

[18] F. Fischer, Z. Naturforsch. **31A**, 302 (1976).

[19] R. J. Atkin and F. M. Leslie, Q. J. Mech. Appl. Math. **23**, S3 (1970).

[20] Routine D02RAF, available through NAG Fortran Library, NAG Central Office, 7 Banbury Rd., Oxford, U.K.

[21] Figure 2 of Cladis and Torza (Ref. 6) for HBAB at 85 °C, when the internal cylinder has radius $R=0.23$ mm, gives a critical velocity $\omega'_c=0.07$ rev/sec, and the equivalent critical velocity for $R=0.16$ mm (the value used in Fig. 1) is $\omega'_c\approx(0.32)0.07/0.16=0.1$ rev/sec. However, the measurements of the velocity profile were obtained at the much

higher value $\omega_1 = 0.6$ rev/sec.
[22]P. K. Currie, G. P. MacSithigh, Q. J. Appl. Math. **32**, 499 (1979).
[23]Routine D02HBF, available through NAG Fortran Library, NAG Central Office, 7 Banbury Rd., Oxford, U.K.
[24]H. Kneppe, F. Schneider, and N. K. Sharma, Ber. Bunsenges. Phys. Chem. **85**, 784 (1981).
[25]H. Kneppe, F. Schneider, and N. K. Sharma, J. Chem. Phys. **77**, 3203 (1982).
[26]P. P. Karat and N. V. Madhusudana, Mol. Cryst. Liq. Cryst. **40**, 239 (1977).
[27]M. J. Bradshaw, D. G. McDonnell, and E. P. Raynes, Mol. Cryst. Liq. Cryst. **70**, 289 (1981).